Korean J. Chem. Eng., 33(8), 2325-2329 (2016)
DOI: 10.1007/s11814-016-0085-7

pISSN: 0256-1115
eISSN: 1975-7220

Photocatalytic activity of metal-decorated SiO_2@TiO_2 hybrid photocatalysts under water splitting

Song Yi Moon*,, Brundabana Naik*,**, and Jeong Young Park*,**,†**

*Center for Nanomaterials and Chemical Reactions, Institute for Basic Science, Daejeon 34143, Korea
**Graduate School of EEWS, Korea Advanced Institute of Science and Technology (KAIST), Daejeon 34143, Korea
(*Received 2 February 2016 • accepted 18 March 2016*)

Abstract−We report the fabrication of a metal-decorated hybrid nanocomposite with TiO_2 encapsulation (Metal/SiO_2@TiO_2, Metal=Pt or Ru) using a simple surface-modification chemical process. Metal nanoparticles capped with polyvinylpyrrolidone were successfully assembled on functionalized SiO_2 via electrostatic interactions, after which a thin layer of TiO_2 was coated on the surface by the sol-gel process to avoid agglomeration of the coated silica spheres. Transmission electron microscopy studies confirmed that the metal nanoparticles were uniformly distributed throughout the surface of the SiO_2 with a thin layer of TiO_2. In addition, X-ray diffraction was employed to ensure the crystal structure of the uniformly coated thin TiO_2 layer. Even after calcination at 500 °C, the structure remained intact, confirming high thermal stability. The photocatalytic activity of the metal-decorated SiO_2/TiO_2 nanocomposites was evaluated using the H_2 evolution reaction. The Metal/SiO_2@TiO_2 catalysts show the photocatalytic water splitting efficiency for H_2 generation (i.e., 0.14% for Pt/SiO_2@TiO_2 and 0.12% for Ru/SiO_2@TiO_2), while there is no generation of H_2 on the Metal/SiO_2 without a coating layer. These results indicate that the anatase crystalline coating layer has good thermal and chemical stability and plays a significant role in photocatalytic H_2 production.

Keywords: Hybrid Nanocomposite, H_2 Evolution, Photocatalytic Activity, Anatase Titania Shell

INTRODUCTION

Hydrogen is considered an important alternative fuel for the future. To produce hydrogen from renewable resources, photocatalytic water splitting under solar light illumination has been studied as an ideal method [1-3]. The use of a semiconductor photocatalyst for water splitting is a promising technique with many advantages [4,5]. In particular, titanium dioxide is preferred due to its outstanding oxidation capability, non-toxicity, high abundance, and convenient band gap (3.2 eV) [6,7]. However, nanosized titania powders with high surface area are not thermally stable [8], and could easily lose their surface area at elevated temperatures through phase transformation and crystallite growth. Therefore, titania is usually coated onto an inert support, such as silica or carbon fibers [9,10].

Many efforts have been made to encapsulate silica with titania to create more accessible photocatalytic sites. Several other studies reported good photocatalytic performance of a titania coating on a silica sphere by changing the physicochemical properties (e.g., crystallinity, crystal size, specific surface area) [11-13]. Niphadkar et al. reported that the TiO_2 in SiO_2/TiO_2 composite materials showed better photoactivity than pure TiO_2 powders due to having a smaller grain size and improved adsorption [14]. The most common synthetic route for coating with TiO_2 is the layer-by-layer (LBL) approach [15,16]. Although the LBL technique shows good control of the size, this process is laborious and time consuming. Alternatively, a simple sol-gel method is more attractive [17,18]. However, the high reactivity of titania precursors leads to several challenges in utilizing the sol-gel approach for titania shell deposition, such as the ease of aggregation of the coated spheres, and the difficulty in forming a regular shell layer with a controlled shell thickness of titania. Liu et al. [19] and Kim et al. [20] controlled the hydrolysis rate of titanium alkoxides to avoid agglomeration of the coated silica spheres [21]; however it is still challenging to achieve a dense, uniform titania coating on the surface of silica spheres via the sol-gel method. In this work, we fabricated silica nanospheres, which serve as an excellent support for nanocrystalline titanium dioxide. We then loaded metal (Pt or Ru) nanoparticles with uniform size on the functionalized silica spheres using electrostatic adsorption. Subsequently, SiO_2@TiO_2 composites with a uniform coating layer were prepared in an aqueous solution via surface modification and the sol-gel process [22,23]. Even after calcination at 500 °C, the structure remained intact, confirming high thermal stability. Similar designs of thermally stable hybrid catalysts composed of nanoparticles with oxide shell or supports have been demonstrated [24,25]. These Metal/SiO_2@TiO_2 (Metal=Pt or Ru) showed enhanced photocatalytic hydrogen production efficiency, compared with pure TiO_2, because of the presence of anatase crystalline TiO_2 metal nanoparticles as the co-catalyst under light irradiation.

EXPERIMENTAL

1. Preparation of Amine-functionalized Silica Nanoparticles

All reagents used were obtained from Sigma-Aldrich without any further purification. Uniform silica with a particle size of 30-

†To whom correspondence should be addressed.
E-mail: jeongypark@kaist.ac.kr

40 nm was prepared via a modified Stöber method [26]. In a typical synthesis, 1.55 ml ammonia ($NH_3 \cdot H_2O$, 27%) was mixed with 4 ml millipore water and 100 ml anhydrous ethanol solution, and then tetraethyl orthosilicate (TEOS, ≥97%) was added. The resultant mixture was stirred for 24 h at room temperature. The suspension was centrifuged at 8,000 rpm and washed with ethanol three times. To functionalize the silica surface with amino groups, the SiO_2 particles were transferred to 40 mL of isopropanol containing (3-aminopropyl) triethoxysilane (APTES, 50 μL) and heated to 80 °C for 2 h [27].

2. Deposition of Metal (Pt and Ru) Nanoparticles on f-SiO_2

To synthesize the 2.7 nm polyvinylpyrrolidone (PVP)-capped Pt nanoparticles, we mixed $H_2PtCl_6 \cdot xH_2O$ and $Pt(acac)_2$ as the precursor; poly(vinylpyrrolidone) and the precursor were added to ethylene glycol in a 50 mL three-necked flask. The mixture was then heated to 200 °C and maintained at this temperature for 10 min under Ar gas. The solution was precipitated with excess acetone and re-dispersed in ethanol [28]. The PVP-capped Ru nanoparticles were prepared via the polyol method in ethylene glycol, as reported previously [29,30]. Metal/f-SiO_2 was synthesized by adding excess PVP-capped nanoparticle colloid (10 ml) to 1.5 ml f-SiO_2 in ethanol under sonication for 30 min. The resulting product was centrifuged and washed three times with ethanol, and then finally dispersed in ethanol (3 ml).

3. Preparation of SiO_2@TiO_2 Nanocomposites Decorated with Metal Nanoparticles

To coat the thin-TiO_2 shell on the Metal/f-SiO_2, the sol-gel process was used. The coating process was performed by hydrolysis of an alkoxide precursor (titanium-butoxide ($Ti(OBu)_4$) in absolute ethanol [31,32]. Typically, 1.5 ml Metal/SiO_2 colloid was dispersed in 10 mL of the ethanol/titanium-butoxide solution by ultrasonic treatment (30 min) and magnetic stirring (30 min), followed by incubation at room temperature for 16 h. The homogeneity of the oxide sol influences the shell thickness. Next, this solution was condensed in ethanol (3 ml) and deionized water (3 ml), and then magnetically stirred for 2 h at room temperature to remove any excess titanium dioxide. The key parameters in homogeneous coating of the silica nanoparticles with TiO_2 are the concentration of $Ti(OBu)_4$ and the amount of time for coating. The coating process was repeated two times. Finally, the coated spheres were washed with water and then ethanol several times, and dried at 80 °C overnight. To obtain an anatase titania shell, the composite particles were calcined at 500 °C for 2 h.

4. Characterization and Photocatalytic Hydrogen Evolution Measurement

The structures and morphologies of the photocatalysts were investigated using transmission electron microscopy (TEM, Tiatan cubed G2 60-300). The crystal phase was studied using an X-ray diffraction spectrometer (XRD, on a Bruker D8 GADDS diffractometer using Co Kα radiation (1.79 Å)). The oxidation states and chemical compositions were measured using a VG Scientific Sigma Probe X-ray photoelectron spectroscopy (XPS) system equipped with an Al Kα X-ray source (1,486.3 eV) under ultra-high vacuum at 10^{-10} Torr. Elemental analyses using inductively coupled plasma mass spectroscopy (PerkinElmer, DRC-e model) were conducted to measure metal loading. The photocatalytic H_2 production reactions were performed in a Pyrex top, irradiation-type vessel connected to a closed gas circulation system at room temperature. A 0.1 g sample was dispersed in an aqueous solution of 10 ml of 10 vol% methanol with 90 mL ultrapure water. The reactant solution was evacuated several times to ensure complete air removal, followed by the introduction of back-filled argon (ca. 5 kPa) into the system. The reaction was initiated by irradiation with a 150 W solar simulator (1.5 AM, 1 sun). The reaction was carried out at a power of 50 mW/cm^2 with an irradiation area of 19.6 cm^2. The evolved gases were analyzed by online gas chromatography (DS Science with a TCD detector and MS-5A column, argon carrier gas). The photocatalytic H_2 evolution activity was estimated from the initial gas evolution rate.

RESULTS AND DISCUSSION

1. Synthesis of Hybrid Nanocatalysts

The detailed synthesis procedure for the Metal/SiO_2@TiO_2 core shell nanocomposites is illustrated in Fig. 1. SiO_2 colloids (30-35 nm in diameter) were functionalized with amine using APTES ((3-aminopropyl)triethoxysilane).

The amine functional groups were necessary for anchoring the metal nanoparticles. We used Pt and Ru nanoparticles capped with PVP (avg. MW=55,000) with an average size of 2-3 nm. NH_2-functionalized SiO_2 spheres were mixed with the metal colloid solution to fabricate the Metal/SiO_2 hybrid photocatalyst. Herein, the metal nanoparticles were anchored to the surface of the f-SiO_2 by electrostatic adsorption; the interactions between the NH_2 group of f-SiO_2 and the metal nanoparticles are well known and reported in the literature [33,34]. Finally, the oxide layer was coated onto the Metal/SiO_2 colloids. This process was accomplished by adding the Metal/SiO_2 solution to an alkoxide solution under incubation and condensation. This facile synthesis strategy avoids various laborious steps, making it highly reproducible and scalable.

2. Metal/SiO_2@TiO_2 Photocatalyst Characterization

Fig. 2(a) and (b) show TEM images of 2-3 nm Pt nanoparticles

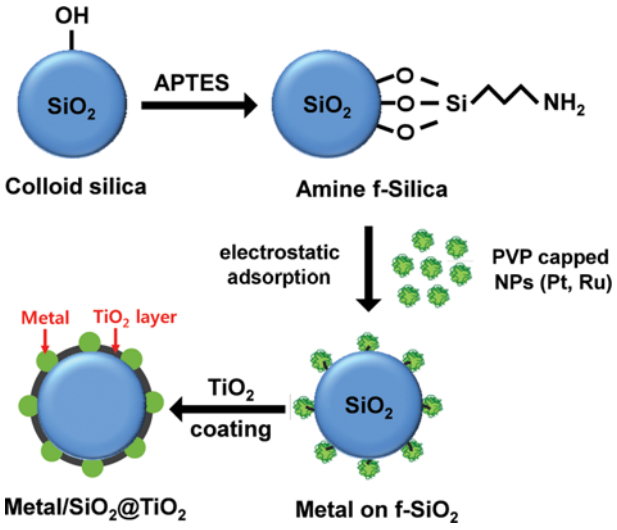

Fig. 1. Schematic diagram of the preparation procedure for the metal/SiO_2@TiO_2 hybrid nanocatalysts (Metal=Pt or Ru).

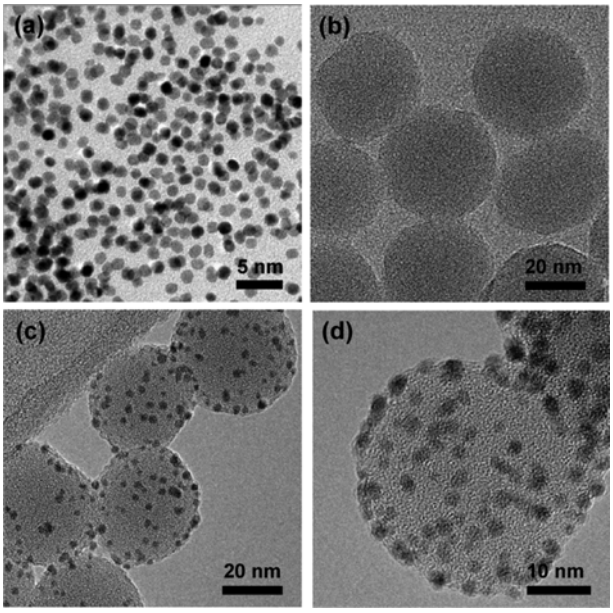

Fig. 2. TEM images of (a) 2.4 nm Pt nanoparticles synthesized through the polyol process, (b) silica spheres used as the core particles, (c) Pt/SiO_2, and (d) Pt/SiO_2/TiO_2.

and the silica nanospheres used as the core particles, respectively. Fig. 2(c) also includes TEM images of the Pt/SiO_2 showing that the metal nanoparticles were finely distributed on the silica sphere (ca. 3 wt% of Pt in the catalyst).

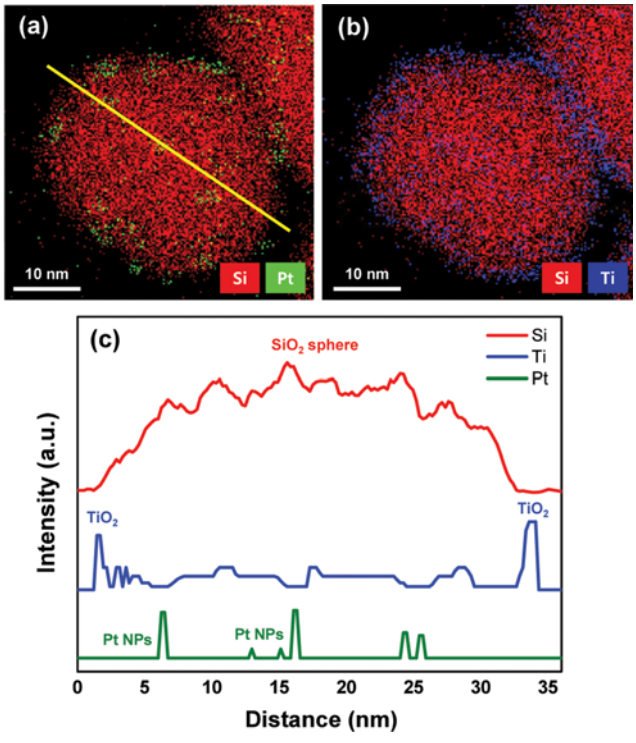

Fig. 3. (a) And (b) phase mapping (Pt is shown in green, Si in red, Ti in blue). (c) EDS line spectra of the Pt/SiO_2@TiO_2 photocatalysts.

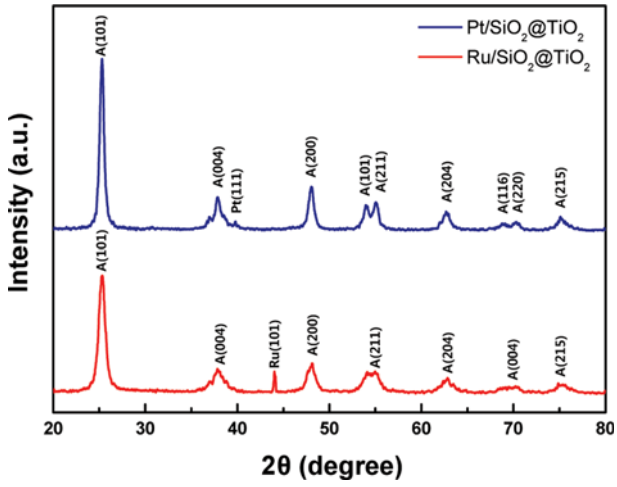

Fig. 4. XRD pattern results of the as-synthesized Pt/SiO_2@TiO_2 and Ru/SiO_2@TiO_2 hybrid catalysts.

It was also confirmed that the metal nanoparticles were spread uniformly on the silica due to the amine groups on the functionalized silica that bind to the capped metal nanoparticles. After oxide coating, the nanocatalysts did not present a considerable change in morphology; a homogeneous and highly dispersed oxide shell is clearly formed (Fig. 2(d)). Phase mapping images of Pt/SiO_2@TiO_2 show that the Pt is well distributed on the SiO_2 support (Fig. 3(a)) and that the TiO_2 layer is uniformly coated on the SiO_2 surface (Fig. 3(b)). In addition, the EDS line spectra clearly demonstrate that the Pt nanoparticles are exposed to the surface and not covered by the oxide layer. To determine the crystalline structure, we performed XRD studies on the titania-coated photocatalysts after calcination at 500 °C for 2 h; the XRD patterns are shown in Fig. 4. Before calcination, we did not observe any diffraction peaks, indicating that the as-prepared titania shell was amorphous. In contrast, the calcined structure exhibited multiple diffraction peaks, which can be indexed to the anatase phase of TiO_2.

The dominant peaks at 2 theta of 25.2°, 37.9°, 48.3°, 53.8°, 55.0°, and 62.7° (i.e., that represent the indices of the (101), (103), (200), (105), (211), and (204) planes, respectively) correspond to the crystalline anatase TiO_2 phase [35]. The presence of the Pt and Ru nanoparticles can be observed by a small diffraction peak at 2 theta of 39.8° and 44.0°, which corresponds to the index of crystalline Pt (111) and Ru (101) planes, respectively [36]. However, the intensity of the peak was quite weak because of the relatively low metal content and high metal dispersion. Moreover, we used X-ray photoelectron spectroscopy to study the influence of the oxidation state of the metal on photocatalytic activity. Fig. 5 shows XPS peaks of the metals; Pt and Ru are mainly present in their respective metallic states. There is also a mixture of oxidized states (+2 and +4 oxidation states) at low concentrations. Ti2p spectra of the Pt/SiO_2@TiO_2 and Ru/SiO_2@TiO_2 catalysts are shown in Fig. 5(b) and (d), respectively, which is characteristic of $Ti2p_{3/2}$ at 458.85 eV and $Ti2p_{1/2}$ at 464.35 eV. These spectra could be deconvoluted into two peaks of Ti^{4+}/TiO_2 and Ti^{3+}/Ti_2O_3.

3. Photocatalytic Activity for Metal/SiO_2@TiO_2

To investigate the effect of the metal nanoparticles and the

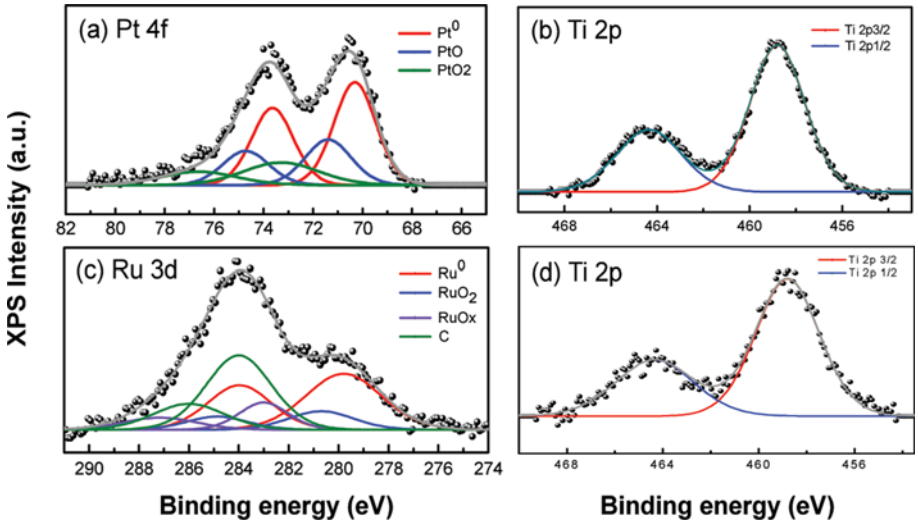

Fig. 5. XPS results of as-synthesized Pt/SiO_2@TiO_2 and Ru/SiO_2@TiO_2 hybrid catalysts. Spectra for (a) Pt4f of Pt/SiO_2@TiO_2, (c) Ru 4f of Pt/SiO_2@TiO_2, and corresponding spectra of Ti2p for (b), (d).

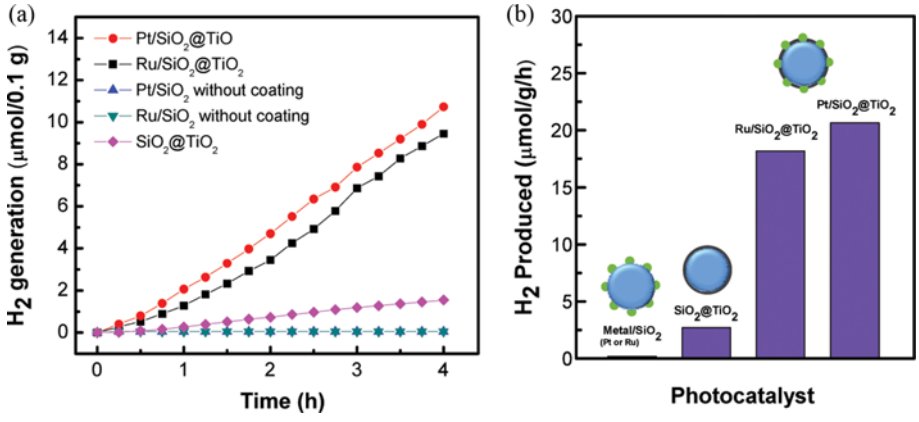

Fig. 6. (a) Time-dependent photocatalytic activity of H_2 generation obtained on Pt/SiO_2@TiO_2 and Ru/SiO_2@TiO_2. (b) Summary of photocatalytic H_2 generation.

oxide shell, photocatalytic H_2 production under simulated solar light was carried out using a 10 volume% methanol solutions as the sacrificial agent over the Metal/SiO_2@TiO_2 photocatalysts. Fig. 6(a) and (b) show the time-dependent photocatalytic activity and a summary of the H_2 generation, respectively. We did not observe H_2 production in the absence of the TiO_2 coating, while the TiO_2-coated catalysts showed enhanced photocatalytic activity (i.e., Pt/SiO_2@TiO_2=20.6 μmol/g/h, Ru/SiO_2@TiO_2=18.2 μmol/g/h). The Metal/SiO_2@TiO_2 photocatalysts showed higher photocatalytic activity than commercial TiO_2-Degussa P25 (6.7 μmol/g/h) [37]. The XRD results reveal that after calcination, the amorphous layer turned into an anatase titania shell, which exhibited significant photocatalytic activity [38].

In other words, the crystallized anatase phase facilitated rapid transfer of photoelectrons from the bulk to the surface, which could effectively inhibit recombination of the photo-generated electrons and holes to improve the photocatalytic activity [39]. In addition, the SiO_2@TiO_2 photocatalyst exhibited lower photocatalytic H_2 generation activity (2.7 μmol/g/h) than the Metal/SiO_2@TiO_2, which demonstrated the role of the noble metal as a co-catalyst for H_2 evolution. Pt nanoparticle deposition can lead to the formation of a Schottky barrier at the interface between the various metals and TiO_2, which could serve as an electron trap to efficiently prevent the electron/hole recombination process [37,40-42]. Especially, through XPS experiments, we identified that the exposed Pt and Ru nanoparticles are mainly present in their metallic states. The presence of a high percentage of metallic nanoparticles acts as a co-catalyst for efficient charge transfer. Consequently, water splitting depends on the physicochemical properties (e.g., crystal size, and dispersion of the titania in the composite) of the catalyst as well as the co-catalyst. The capability of synthesizing well-defined crystalline titania-coated silica particles can open up new opportunities in many applications, including solar cells and photocatalytic decomposition of pollutants.

CONCLUSION

We successfully synthesized Metal/SiO_2@TiO_2 (Metal=Pt or Ru)

hybrid photocatalysts and demonstrated using different analytical techniques (TEM, XRD, and XPS) that this novel catalyst design is encapsulated with a uniform TiO_2 layer. We investigated the role of the crystalline oxide coating layer in photocatalytic water splitting efficiency to generate H_2. The measured solar energy conversion efficiencies are 0.14% for Pt/SiO_2@TiO_2 and 0.12% for Ru/SiO_2@TiO_2, respectively, while there is no generation of H_2 on Pt/SiO_2 without a coating layer. The enhanced photocatalytic activity is attributed to the anatase crystallinity of the TiO_2. The presence of Pt at the surface results in the formation of a Schottky barrier at the metal-oxide interface, which facilitates interfacial electron transfer and subsequently encourages charge carrier separation. As a result, the transfer of charge carriers is remarkably improved, which in turn results in enhanced photocatalytic H_2 generation.

ACKNOWLEDGEMENT

This work was supported by IBS-R004-G4.

REFERENCES

1. R. M. Navarro, M. A. Pena and J. L. G. Fierro, *Chem. Rev.*, **107**, 3952 (2007).
2. B. Naik, S. M. Kim, C. H. Jung, S. Y. Moon, S. H. Kim and J. Y. Park, *Adv. Mater. Interfaces*, **1**, 1300018 (2014).
3. A. Kudo and Y. Miseki, *Chem. Soc. Rev.*, **38**, 253 (2009).
4. B. Naik, S. Martha and K. M. Parida, *Int. J. Hydrogen Energy*, **36**, 2794 (2011).
5. M. R. Hoffmann, S. T. Martin, W. Y. Choi and D. W. Bahnemann, *Chem. Rev.*, **95**, 69 (1995).
6. A. L. Linsebigler, G. Q. Lu and J. T. Yates, *Chem. Rev.*, **95**, 735 (1995).
7. X. Chen and S. S. Mao, *Chem. Rev.*, **107**, 2891 (2007).
8. J. W. Lee, M. R. Othman, Y. Eom, T. G. Lee, W. S. Kim and J. Kim, *Micropor. Mesopor. Mater.*, **116**, 561 (2008).
9. N. Rungjaroentawon, S. Onsuratoom and S. Chavadej, *Int. J. Hydrogen Energy*, **37**, 11061 (2012).
10. F. Tian, Z. S. Wu, Y. J. Yan, X. Y. Ge and Y. B. Tong, *Korean J. Chem. Eng.*, **32**, 1333 (2015).
11. D. J. Reidy, J. D. Holmes and M. A. Morris, *Ceram. Int.*, **32**, 235 (2006).
12. K. Wang, Y. X. Chen and F. X. Ye, *Chinese J. Catal.*, **25**, 931 (2004).
13. S. Alijani, A. Z. Moghaddam, M. Vaez and J. Towfighi, *Korean J. Chem. Eng.*, **30**, 1855 (2013).
14. P. S. Niphadkar, S. K. Chitale, S. K. Sonar, S. S. Deshpande, P. N. Joshi and S. V. Awate, *J. Mater. Sci.*, **49**, 6383 (2014).
15. P. Wilhelm and D. Stephan, *J. Colloid Interface Sci.*, **293**, 88 (2006).
16. H. Nakamura, M. Ishii, A. Tsukigase, M. Harada and H. Nakano, *Langmuir*, **21**, 8918 (2005).
17. D. P. Wang and H. C. Zeng, *Chem. Mater.*, **21**, 4811 (2009).
18. P. Wilhelm and D. Stephan, *J. Photochem. Photobiol. A.*, **185**, 19 (2007).
19. L. X. Liu, P. Dong, R. X. Liu, Q. Zhou, X. D. Wang, G. Y. Yi and B. Y. Cheng, *J. Colloid Interface Sci.*, **288**, 1 (2005).
20. K. D. Kim, H. J. Bae and H. T. Kim, *Colloids Surf., A.*, **221**, 163 (2003).
21. H. Nakamura, M. Ishii, A. Tsukigase, M. Harada and H. Nakano, *Langmuir*, **22**, 1268 (2006).
22. B. Naik, S. Y. Moon, S. Oh, C. H. Jung and J. Y. Park, *Catal. Lett.*, **145**, 930 (2015).
23. A. S. Reddy, S. Kim, H. Y. Jeong, S. Jin, K. Qadir, K. Jung, C. H. Jung, J. Y. Yun, J. Y. Cheon, J. M. Yang, S. H. Joo, O. Terasaki and J. Y. Park, *Chem. Commun.*, **47**, 8412 (2011).
24. J. Yun, C. H. Jung, D. Park, H. Y. Koo, J. Y. Yun, Y. Kim and J. Y. Park, *Korean J. Chem. Eng.*, **31**, 1980 (2014).
25. S. H. Joo, J. Y. Park, C. K. Tsung, Y. Yamada, P. D. Yang and G. A. Somorjai, *Nature Mater.*, **8**, 126 (2009).
26. Y. Kobayashi, H. Katakami, E. Mine, D. Nagao, M. Konno and L. M. Liz-Marzan, *J. Colloid Interface Sci.*, **283**, 392 (2005).
27. K. Gude and R. Narayanan, *J. Phys. Chem. C*, **114**, 6356 (2010).
28. R. M. Rioux, H. Song, J. D. Hoefelmeyer, P. Yang and G. A. Somorjai, *J. Phys. Chem. B*, **109**, 2192 (2005).
29. S. H. Joo, J. Y. Park, J. R. Renzas, D. R. Butcher, W. Y. Huang and G. A. Somorjai, *Nano Lett.*, **10**, 2709 (2010).
30. K. Qadir, S. H. Joo, B. S. Mun, D. R. Butcher, J. R. Renzas, F. Aksoy, Z. Liu, G. A. Somorjai and J. Y. Park, *Nano Lett.*, **12**, 5761 (2012).
31. S. H. Lim, N. Phonthammachai, S. S. Pramana and T. J. White, *Langmuir*, **24**, 6226 (2008).
32. K. An, S. Alayoglu, N. Musselwhite, K. Na and G. A. Somorjai, *J. Am. Chem. Soc.*, **136**, 6830 (2014).
33. D. Wen, S. J. Guo, J. F. Zhai, L. Deng, W. Ren and S. J. Dong, *J. Phys. Chem. C*, **113**, 13023 (2009).
34. R. G. Freeman, K. C. Grabar, K. J. Allison, R. M. Bright, J. A. Davis, A. P. Guthrie, M. B. Hommer, M. A. Jackson, P. C. Smith, D. G. Walter and M. J. Natan, *Science*, **267**, 1629 (1995).
35. M. Hussain, M. Ahmad, A. Nisar, H. Y. Sun, S. Karim, M. Khan, S. D. Khan, M. Iqbal and S. Z. Hussain, *New J. Chem.*, **38**, 1424 (2014).
36. Y. S. Kim, H. I. Kim, M. A. Dar, H. K. Seo, G. S. Kim, S. G. Ansari, J. J. Senkevich and H. S. Shin, *Electrochem. Solid. St.*, **9**, C19 (2006).
37. B. Naik, S. Y. Moon, S. H. Kim and J. Y. Park, *Appl. Surf. Sci.*, **354**, 347 (2015).
38. K. Kato, A. Tsuzuki, H. Taoda, Y. Torii, T. Kato and Y. Butsugan, *J. Mater. Sci.*, **29**, 5911 (1994).
39. R. Y. Zhang, D. K. Shen, M. Xu, D. Feng, W. Li, G. F. Zheng, R. C. Che, A. A. Elzatahry and D. Y. Zhao, *Adv. Energy Mater.*, **4**, 130175 (2014).
40. B. K. Vijayan, N. M. Dimitrijevic, J. S. Wu and K. A. Gray, *J. Phys. Chem. C*, **114**, 21262 (2010).
41. K. C. Goddeti, S. M. Kim, Y. K. Lee, S. H. Kim and J. Y. Park, *Catal. Lett.*, **144**, 1411 (2014).
42. J. Y. Park, L. R. Baker and G. A. Somorjai, *Chem. Rev.*, **115**, 2781 (2015).